Eur. Phys. J. E (2015) **38**: 85
DOI 10.1140/epje/i2015-15085-4

THE EUROPEAN PHYSICAL JOURNAL E

Regular Article

Computational study of remodeling in a nucleosomal array

Raoul D. Schram[1], Henrike Klinker[2], Peter B. Becker[2], and Helmut Schiessel[1,a]

[1] Instituut-Lorentz, Leiden University, P.O. Box 9506, 2300 RA Leiden, The Netherlands
[2] Adolf-Butenandt-Institute and Center for Integrated Protein Science Munich, Ludwig-Maximilians-University, Munich, Germany

Received 9 January 2015 and Received in final form 18 May 2015
Published online: 10 August 2015 –

Abstract. Chromatin remodeling complexes utilize the energy of ATP hydrolysis to change the packing state of chromatin, *e.g.* by catalysing the sliding of nucleosomes along DNA. Here we present simple models to describe experimental data of changes in DNA accessibility along a synthetic, repetitive array of nucleosomes during remodeling by the ACF enzyme or its isolated ATPase subunit, ISWI. We find substantial qualitative differences between the remodeling activities of ISWI and ACF. To understand better the observed behavior for the ACF remodeler, we study more microscopic models of nucleosomal arrays.

1 Introduction

Eukaryotic DNA molecules are wrapped around millions of protein cylinders. In each complex, called nucleosome, 147 base pairs (bp) are wrapped tightly along a left-handed superhelical path around an octamer of histone proteins [1]. This raises the question of how DNA can be accessed and read out. There are two possibilities to achieve this, namely the DNA wrapped in a nucleosome can be freed by thermal fluctuation or via active ATP-consuming processes [2]. Well-known passive processes are site exposure through partial DNA unspooling [3–12] and nucleosome sliding along the DNA molecule [13–18]. The latter process is caused by defects in the wrapped DNA molecule [19, 20], most likely bulges [21, 22] or twist defects [23–25]. As nucleosome sliding is very slow, the necessity for active processes is evident. Towards this end a large variety of ATP-consuming protein machines, called chromatin remodelers, exist that can catalyse the sliding of histone octamers along the DNA molecule or the partial (or complete) disassembly of nucleosomes [26–29].

ACF-type remodelers will not disrupt nucleosome fibres, but rather slide nucleosomes to convert irregular successions of nucleosomes into regular arrays with defined nucleosome spacing [30–35]. This might be one of the mechanisms where a higher-order structure has an impact on gene regulation in cells [36]. For instance, the results of a recent quantitative theoretical study [37] suggest that only arrays with equally spaced nucleosome can fold into a chromatin fiber. Recently, synthetic arrays bearing up to 26 nucleosomes have been monitored [38, 39]. In this paper we analyze experimental data obtained in the context of the latter study [39]. We have results from two types of remodelers from *Drosophila*. One is the aforementioned ACF remodeler, which consists of the ATPase ISWI and an ACF1 subunit, and the other is ISWI alone. The association of ACF1 with ISWI changes the directionality of nucleosome sliding by ISWI on short DNA fragments [40, 41].

In the experiment analyzed here, nucleosomes are initially positioned at equal distance from each other through repeats of a strong DNA positioning sequence ("Widom-601"; [42]), see fig. 1(a). A reaction is set up containing the nucleosomal array, ATP and the AluI restriction enzyme. The enzyme cuts specifically at only one site per repeat, which is initially located 43 bp inside each of the wrapped DNA portions of each nucleosome. Thus none of the AluI sites are easily accessible at the start of the experiment. At time $t = 0$ the remodeling enzyme is added. Restriction recognition sites now become accessible through the remodeling of the nucleosomes, as these get shifted out of the way. At certain time points the sample is analyzed by separating DNA fragments by their length through gel electrophoresis, fig. 1(b). Visible are only those fragments that contain one of the two ends of the original DNA molecule to which a fluorescent label was attached. Thus rather indirectly, the intensity of the different bands in the gel contain information about the cutting rates of each individual restriction site, and through that information about the activity of the remodeler itself.

In this paper we attempt to extract this information. In sect. 3 we introduce models that are as simple as possible but still can describe the data. In sect. 4 we present

[a] e-mail: schiessel@lorentz.leidenuniv.nl

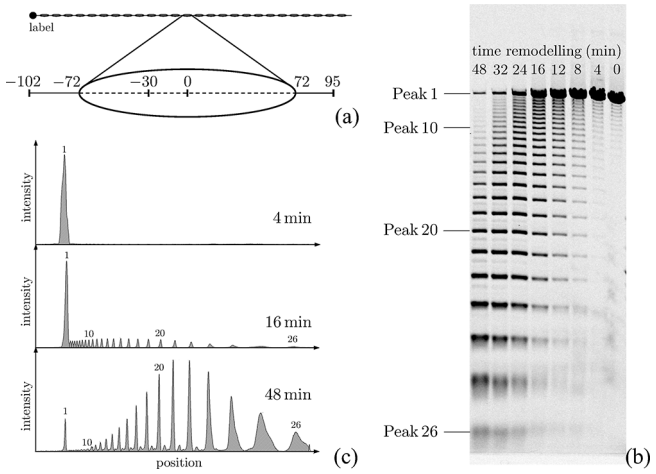

Fig. 1. (a) Schematic depiction of the nucleosome array. Nucleosome positions are indicated by ellipses. The array DNA comprised 26 repeats of a 197 bp fragment (magnification) containing the Widom-601 nucleosome positioning sequence (dashed line). Numbers indicate the positions of the restriction enzyme site and the nucleosome boundaries with respect to the nucleosomal dyad axis (0). (b) Example of a gel picture obtained from a remodeling experiment with ISWI. Peak 26 is the fastest moving band, corresponding to a single nucleosome, peak 1 contains the full array. Different lanes correspond to different remodeling times, as indicated on top. (c) Peak profiles obtained from the gel in (b) after 4, 16 and 48 minutes of remodeling. The intensity is plotted as a function of position (both axes arbitrary units).

the results and discuss how these findings can be interpreted with the help of more microscopic models. Finally, we present our conclusions in sect. 5.

2 Experiment

Fluorescently labeled nucleosome arrays and remodeling enzymes were prepared as described previously [39]. The remodeling assays were performed as detailed in [39] with limiting remodeling enzyme concentrations. The restriction enzyme is added at the very beginning of the experiment, along with the remodeling factor, as has been done in the cited reference. It is added in excess so that cleavage is only limited by nucleosome occupancy and any site exposure will immediately be scored by cleavage (see refs. [3, 43–46] for other examples where restriction enzyme sensitivity is used as a stringent and quantitative assay for nucleosome DNA accessibility). After size separation in agarose gels (see fig. 1(b) for an example with ISWI), the labeled DNA fragments were quantified using the AIDA software (1D evaluation; raytest), see fig. 1(c). Thereby, gel lanes were identified and the borders of the peaks representing individual DNA bands were assigned manually. Signal intensity of gel regions above the highest and below the lowest DNA band was considered as background.

The number of experiments analyzed is 4 in the case of the ISWI remodeler and 5 for ACF. Ideally, at $t = 0$, there is only one fragment length in the system (26) corresponding to peak 1. In practice there is a small amount of fragments with shorter lengths present. Peaks close to peak 1, however, cannot be detected. In our simulations we take this into account through the initial conditions, and choose for those hidden peaks the same value as for the first visible peak next to peak 1.

3 Models

We use two different models, a simple one for the ISWI protein and a more complex one for the ACF remodeler. Here we define the model before we apply it to the experimental data in the next section. The kinetics of cleavage is two orders of magnitude faster than the remodeling process itself, and for the purposes of the modeling, is considered instantaneous as soon as the site is exposed.

3.1 ISWI model

Our ISWI model is the simpler of the two models described here. We assume that each AluI site is cut with equal rate, independently of whether other AluI sites on the fragment are cut or not. The corresponding probability distribution of the time before a cut is based on the fact that remodeling itself consists of several discrete steps. Therefore we do not expect the duration of a remodeling step to be exponentially distributed. Since we have no *a priori* information about the shape of this distribution, we choose a fairly generic one, namely the Poisson distribution:

$$P(\text{cut at } t) = \lambda^{k+1} t^k \exp(-\lambda t)/k!. \tag{1}$$

This is equivalent to k independent steps with an exponential distribution. The number of "steps" k and the overall rate λ of a single step are free parameters of the model. The best fit to the experimental data was found when we use $k = 3$.

From this we infer that the true underlying distribution is most likely not exponential. On the very basic level, a value of $k > 1$ shows an important feature of the remodeling process, namely that it has memory. This reflects the presence of either substeps within a remodeling step, or various remodeling steps needed for nucleosomes, before their AluI sites are exposed, or a combination of both.

3.2 ACF model

The ISWI model described above produces only poor fits to the experimental ACF data. We achieve a dramatic improvement through the addition of one extra feature: the number of steps before a restriction enzymes cuts a site is biased towards one end. We find that restriction sites closer to the end containing the fluorescent label need on average fewer steps and thus are typically cut before those close to the other end. Since the number of steps is discrete and relatively small, the bias is applied in the

Table 1. Difference matrix between the remodeling experiments. Lower values indicate that the two experiments are more similar. It is apparent from the table that the ISWI and ACF experiments behave differently, as the difference between them is always higher than comparisons between experiments of the same kind. The number presented in the table is $\langle|\log(I_{\exp_A}/I_{\exp_B})|\rangle$ (with some small adjustments explained in the main text). Values below 0.2 indicate excellent agreement, while values below 0.3 can often be considered quite adequate still.

	ISWI 1	ISWI 2	ISWI 3	ISWI 4	ACF 1	ACF 2	ACF 3	ACF 4	ACF 5
ISWI 1	0	0.140	0.425	0.446	0.738	0.504	0.608	0.561	0.643
ISWI 2	0.140	0	0.235	0.236	0.603	0.467	0.539	0.440	0.510
ISWI 3	0.425	0.235	0	0.316	0.743	0.445	0.746	0.556	0.633
ISWI 4	0.446	0.236	0.316	0	0.606	0.475	0.563	0.402	0.512
ACF 1	0.738	0.603	0.743	0.606	0	0.142	0.225	0.250	0.152
ACF 2	0.504	0.467	0.445	0.475	0.142	0	0.232	0.148	0.099
ACF 3	0.608	0.539	0.746	0.563	0.225	0.232	0	0.294	0.222
ACF 4	0.561	0.440	0.556	0.402	0.250	0.148	0.294	0	0.151
ACF 5	0.643	0.510	0.633	0.512	0.152	0.099	0.222	0.151	0

form of a probability p for each additional step beyond one:

$$p(j) = (j/L)^{\beta}, \tag{2}$$

where β is a bias exponent and j is the restriction site number, $1 \leq j \leq L$ with $L = 26$ being the number of nucleosomes of the full template. We denote with $j = 1$ the restriction site closest to the fluorescent label. At the start of each simulation run, the number of steps for each restriction site is determined as follows. For each site we draw N_p random numbers $U_i \in [0, 1)$. The number of steps is then 1 plus the count of random numbers that are less than $p(j)$. Thus the number of steps is at least one and never bigger than N_p+1. Since we execute 100000 runs per simulation, the distribution is smoothed out. The variable N_p is adjusted by hand, namely several points surrounding the optimum are compared and the one that brings the best solution is selected. We found the best value to be $N_p = 1$. This mean that we get for each run a set of 1's and 2's for the restriction sites. The realization of these 1's and 2's is different for each run.

3.3 Data analysis

After manually setting $k = 3$ (for the ISWI case) or $N_p = 1$ (for the ACF case), there are one (for the ISWI case) or two (for the ACF case) additional free parameters in our system: the reaction rate λ and, for the ACF model, the bias exponent β, governing the average number of steps required along the nucleosomal array, see eq. (2). The parameter λ is found for each experimental sample individually using the search algorithm described below.

First we define our objective function to be minimized, namely

$$d(\mathrm{sim}, \mathrm{exp}) = \langle|\log(I_{\mathrm{exp}}/I_{\mathrm{sim}})|\rangle. \tag{3}$$

Here the average $\langle\cdot\rangle$ is taken over all experimental time points and fragment lengths. I_{exp} and I_{sim} are the abundances of, respectively, the experimental and simulation data, at certain time points and fragment lengths. The choice was made to work with logarithms, because —by the nature of the problem— intensities tend to decay (pseudo-) exponentially, and we would like to take all time points equally into account. The same comparison can also be done between two simulations or two experiments. In the latter case, only time points and fragment lengths that both sets have in common are taken into account. A comparison between the various remodeling experiments is presented in table 1.

There are some exceptions to the computation of the terms given by eq. (3). If the experimental value for the normalized peak intensity is below the threshold 10^{-3}, it is considered to be indistinguishable from 0. If the simulation also gives a value below that threshold, the match is considered perfect and it adds 0 to the average. In the case that the simulation predicts an intensity higher than the threshold, the deviation added to the sum is equal to $\log(I_{\mathrm{sim}}/I_{\mathrm{thres}})$. If the experiment gives a value above the threshold and the simulation gives a value below the threshold, the calculation is done with $I_{\mathrm{sim}} = I_{\mathrm{thres}}$. This is done to prevent a very small value for the simulation from dominating the final error d.

The search algorithm to find optimal values for the free parameters starts with a predefined search range. Then five points (for ISWI) or a 5×5 point grid (for ACF) are chosen at equal distances within this range. For all these points the objective function is evaluated, by performing a simulation run with the corresponding parameter value(s). The next iteration is done within a range half as large and centered around the point with the best objective value. After a couple (5) of iterations, the search is stopped, and the parameters with the best objective value d are presented.

4 Results and discussion

4.1 ISWI protein

The ISWI case seems rather straightforward as we have only 2 adjustable parameters, k and λ, in our simple

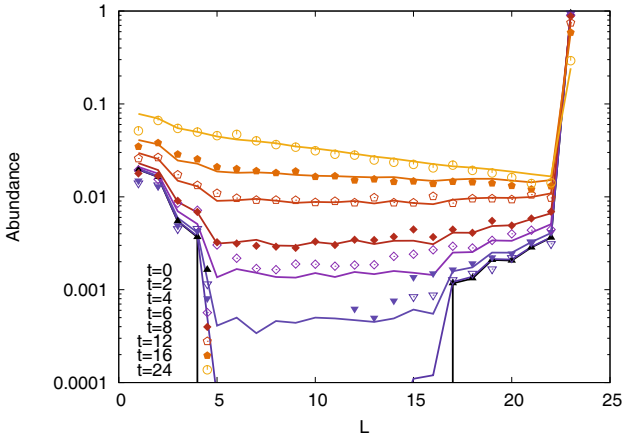

Fig. 2. Example of a fit of the model simulation (lines) to the experimental data (symbols) for remodeling with ISWI. The x-axis represents the fragment length, while the y-axis shows the relative peak intensity ($I/I_{\rm tot}$), at different time points given in minutes.

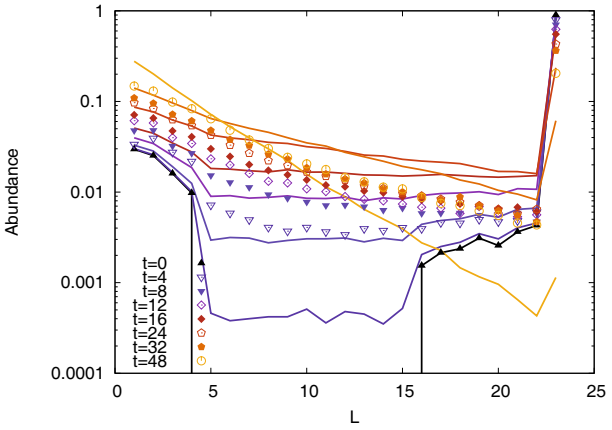

Fig. 3. Example of a fit of the ISWI model (lines) to the ACF remodeling experiment (symbols). The x-axis represents the fragment length, while the y-axis shows the relative peak intensity ($I/I_{\rm tot}$), at different time points given in minutes. The model treats all the nucleosomes along the array equally which leads to a very poor fit.

model. We obtain a decent agreement with the experimental data when choosing $k = 3$ and an appropriate value for λ. It is, however, unfortunate that there is a lot of sample to sample variation. There is an average difference of 0.299 between the samples. On the other hand, the average difference between the model (with one single set of parameters for all experiments) and the experiment is lower, $d = 0.257$, with the rate given by $\lambda = 0.0126$. Although counterintuitive, the objective function is actually expected to be higher for the inter-experimental differences than for the comparison between simulation and experiment. The reason for this is that the starting conditions for the experiments are slightly different for each sample, and this is accounted for in the simulation. We have checked that the choice $k = 3$ is indeed optimal. For the two neighboring choices we have: $k = 2$: $d = 0.294$ and $k = 4$: $d = 0.474$.

Figure 2 shows the comparison between experiment and simulation for the first sample, ISWI 1. For this sample the agreement is excellent. Here the best parameters for only this single experiment are used.

We conclude that there is no indication of a significant bias in the cutting probabilities as one goes along the chain of nucleosomes.

4.2 ACF remodeler

The ACF model brings in a new parameter, β. The value found for β does not seem to be zero, which at first is quite surprising. If we use the ISWI model (which corresponds to the ACF model with $N_p = k - 1 = 2$, and $\beta = 0$), we get a very poor fit to the experimental data ($d = 0.671$). As an illustration we have plotted in fig. 3 the comparison for the first set of experimental data (ACF 1).

In the case of the ACF enzyme, the inter-experimental differences are fortunately much smaller than in the ISWI case, namely 0.173 on average. This is also reflected in the quality of the fit of our simulation to the data with an average $d = 0.157$. The best set of parameters for all experimental data was found to be $\lambda = 0.0022$ and $\beta = 0.375$, with $N_p = 1$. In fig. 4 a comparison between one particular experiment, ACF 1, and the simulation is shown. Again we attempted a neighboring choice with $N_p = 2$, which gives a difference $d = 0.256$.

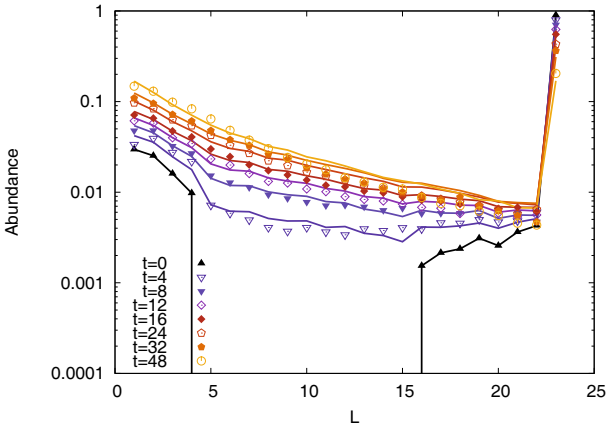

Fig. 4. Same as fig. 3 but this time allowing for a remodeling bias along the nucleosomal array according to eq. (2).

To achieve a satisfying fit between the model and the ACF data we needed to use a non-vanishing value of β. This suggests that the cutting probabilities change along the nucleosomal array. In the next section we discuss possible mechanisms that could cause this effect.

4.3 Asymmetry in the cutting probabilities

The DNA digestion data for ACF remodeling suggest that the accessibility for restriction enzymes to the AluI sites varies along the nucleosomal array. There are two main asymmetries in the system. The first one is the presence of the fluorescent label on one end of the DNA molecule,

but not on the other. This might cause an asymmetry in the data due to some interaction between the label and the remodeler (or the restriction enzyme) that makes it more likely to remodel (or cut) close to the label. Interactions of an SF2 helicase and even ISWI itself with fluorophores at DNA ends have indeed been observed before [47,48].

Another possibility is that the asymmetry stems from the asymmetric positions of the AluI restriction sites with respect to the nucleosomal footprints. The sites are not positioned at the initial centers of the nucleosomal DNA stretches, but sit away from the centers towards the labeled end. Thus, remodeling away from the label is more likely to expose an AluI site than the reverse, because less steps need to be taken for exposure. Additionally, the probability distribution of the nucleosome positions is not simply periodic due to end effects but shows a decay of the oscillations as one moves away from fixed boundaries [49]. In addition, the distributions of end nucleosomes (and of the ones close to it) are skewed since the boundary is fixed whereas the array of the nucleosomes on the other side constitute effectively a soft boundary. As only fragments are detected in the experiment if they contain the labelled end and as the nucleosome distribution is skewed to fluctuate away from ends, we expect that AluI sites close to the label are easier to access than sites that are further away from it.

To provide more concrete evidence for these claims, we performed a number of simulations. The first set of simulations finds the equilibrium or steady state accessibility for different models. The second part uses more detailed models to try and fit the experimental data. In all the models we use the same size for the DNA molecule as in the experiments. There is an 8 bp long head at the labelled end, 26 repeats of length 197 bp and a 20 bp long tail leading to a total length of 5150 bp. The first AluI site is positioned at bp 81. The initial position of the first nucleosome is at 36 bp. In all simulations, the nucleosome covers 147 bp and nucleosomes are not allowed to overlap. We neglect here any effects due to sequence specific mechanical properties of the DNA molecule [50], *i.e.* we assume that the chromatin remodelers override sequence specificity [51].

4.3.1 The Tonks gas model

The most simple way to describe the conformation of a nucleosomal array is the Tonks gas, one-dimensional discs on a one-dimensional line with steric hard core interactions [52], see also refs. [49, 53]. For simplicity we consider here equilibrium statistics, which makes the dynamics unimportant for the results. At each step we select a nucleosome randomly with equal probability, and a random direction (left or right) as well, with a step size of 1. The move is accepted if the moved nucleosome does not overlap with another nucleosome or does not fall off at either end. The system is first thermalized for 10^7 steps, and then sampled for another 10^9 steps.

Figure 5 shows the accessibility as a function of the bp number (starting from the label at 0). The accessibility

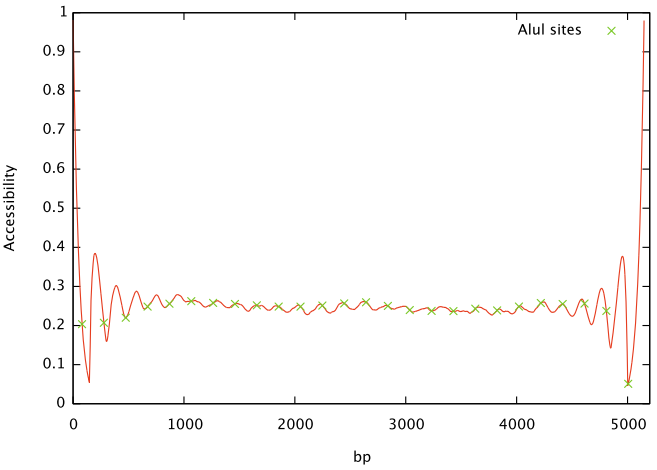

Fig. 5. Accessibility plotted as a function of the bp number for the Tonks gas model (the label is at position 0). The DNA molecule has the same number of repeats (26) and base pairs as in the experiments with the ISWI and ACF remodelers. The green symbols denote the accessibilities to the AluI sites.

to a base pair is defined as the fraction of time the site is not under a nucleosome, *i.e.* it is given by one minus the probability that this base pair is occupied by a nucleosome. We find strong oscillations at the boundaries that decay as one moves away from the ends toward the center, consistent with what has been reported by Kornberg and Stryer [49]. But since the AluI restriction sites are not positioned symmetrically, the accessibility to these sites (indicated by crosses in fig. 5) are not symmetrical with respects to the two ends of the array.

Note, however, that there is no clear trend with respect to the two ends. Unlike what we suggested above and what we used in our modeling of the ACF data, we do not detect an overall tendency that the accessibility to the restriction sites is higher close to the labeled end. However, this model does not include the well-known property of the ACF remodeler to create arrays of equally spaced nucleosomes [31–33]. In that sense the model is more appropriate to describe the ISWI data. In fact, we found in this paper that we could model the ISWI data in a satisfactory way by assuming that cutting probabilities for all restriction sites are identical.

4.3.2 Semi-soft sphere model

To account for the spacing property of the ACF remodeler, we modified the model to have (semi) soft spheres instead of hard spheres. The nucleosomes themselves are still not allowed to overlap, but we assume an additional repulsive force between neighboring nucleosomes with a maximum range of 60 bp. To model this repulsion, our model consists of an alternating series of rods (the nucleosomes) and harmonic springs with 60 bp rest lengths. The springs are not attached to the rods, so the interaction is switched off beyond that length. This accounts for the observation that ACF-catalyzed nucleosome movements toward a barrier

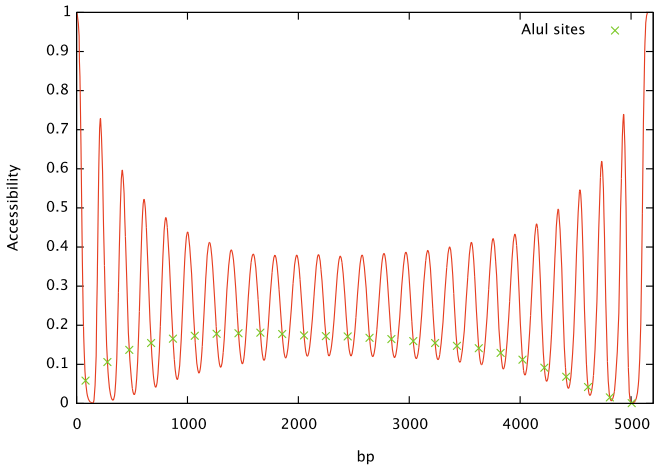

Fig. 6. Accessibility plotted as a function of the bp distance from the label for the semi-soft sphere model. Same system as in fig. 5 but the sphere have in addition to the 147 bp hardcore a soft shell with an extra 30 bp on either side.

are as fast as away from it once the linker length exceeds $l_{\max} = 60$ bp [31]. The interaction between the two neighboring nucleosomes labeled i and $i+1$ is thus given by

$$E(i, i+1) = \begin{cases} (d_{i,i+1} - l_{\max})^2 & \text{if } d \leq l_{\max}, \\ 0 & \text{else}, \end{cases} \quad (4)$$

where $d_{i,i+1}$ is the distance between nucleosomes i and $i+1$ (always larger than zero). The interaction between the DNA terminus and the corresponding end nucleosome is modeled as if there is a static nucleosome sitting just at the DNA end.

The accessibility for the semi-soft sphere model is shown in fig. 6. It shows oscillations with a much higher amplitude than in the case of the Tonks gas (see fig. 5). This reflects the fact that springs cause a more defined positioning of the nucleosomes. Remarkably, the accessibility to the AluI restriction sites shows a clear asymmetry. Going from left to right the accessibility increases for the first 9 nuclesomes but then decreases systematically for the next 17 nucleosomes. Even though the accessibility follows not the same functional form as in eq. (2) it shows overall the same tendency, namely a higher accessibility to the restriction sites on the side closest to the label.

4.3.3 A dynamic model

Finally we implemented the more precise model described in ref. [35]. In this model the nucleosomes move in steps of 13 bp. The rate of a step where nucleosomes i and $i+1$ move towards each other is determined by the following equation:

$$r_{i,i+1} = \begin{cases} 0 & \text{if } d_{i,i+1} \leq l_{\min}, \\ \lambda_r \exp(b(d_{i,i+1} - l_{\max})) & \text{if } l_{\min} < d_{i,i+1} \leq l_{\max}, \\ \lambda_r & \text{if } d_{i,i+1} > l_{\max}, \end{cases} \quad (5)$$

where the parameters $l_{\max}$ (as above), $l_{\min}$ and b are directly determined from the experiments [35]. At each step a move is selected with a probability proportional to its rate.

In view of the more detailed nature of the model, we also refined the definition of accessibility. We know from experiments that base pairs are accessible even inside a nucleosome albeit at a reduced rate. This is caused by a process called site exposure where the DNA temporarily unspools from the protein core as mentioned in the introduction. This has in fact been shown by measuring the reduced accessibility of restriction enzymes to their target sites inside nucleosomes [3]. Theoretical modeling [10] suggests in addition that the restriction sites are less accessible when within a 30 bp distance from the entrance point to the nucleosome (see fig. 3 in that reference). According to ref. [10] the accessibility to the restriction site is to a good approximation given by

$$p_{\text{open}} = \min\{1, \exp((d-30)/10)\}, \quad (6)$$

where d is the distance from the closest edge of a nucleosome (in bp and counted positive if outside and negative if inside the nucleosome).

The simulation uses rejection-free sampling with the corresponding time differences Δt between events given by

$$\Delta t = \frac{1}{\sum r_i}, \quad (7)$$

where r_i are the rates of all events that can take place at a certain point in time. Thus, Δt is not constant in time and depends on the configuration itself.

The result for the accessibility in the steady state are presented in fig. 7. The picture looks qualitatively similar to the soft-sphere model, see fig. 6. This suggests that details of the microscopic model do not influence the accessibility qualitatively, but can have a quantitative effect. Unfortunately none of our microscopic models showed a power law for the accessibility distribution that we assumed in our ACF model above (see eq. (2)) and that worked well to fit the ACF data (see fig. 4).

We finally attempted to model the actual time development of the system. This is in principle possible, since the starting positions of the nucleosomes are known experimentally (given by the Widom-601 positioning sequences). It is just a matter of taking the accessibility rates at the requested time points and comparing them to the experimental data. There are two free parameters in the model: one is the remodeling rate λ_r. The other one is the cutting rate λ_c. The accessibility is expected to be relatively low, because of the regular spacing mechanism of the ACF remodeler. Therefore, the distribution of the time to remodel (or cut) is less important. Thus, we decided to take always the average time to cut or remodel, and not the actual distribution (since it is unknown anyway). Note that the time between two remodeling steps is still a distribution (non-deterministic), because probabilities of the steps that are taken depend on the rates $r(t, i, i+1)$, with the actual steps being chosen randomly according to their rate.

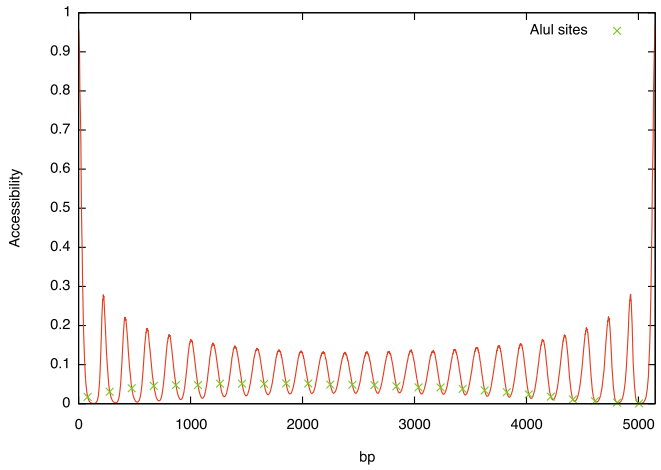

Fig. 7. Accessibility plotted as a function of the bp distance from the label for the steady state of our dynamical model. The model accounts for experimentally measured details both for the ACF remodeling activity and for the accessibility of restriction enzymes to base pairs close to or inside nucleosomes (see text for details).

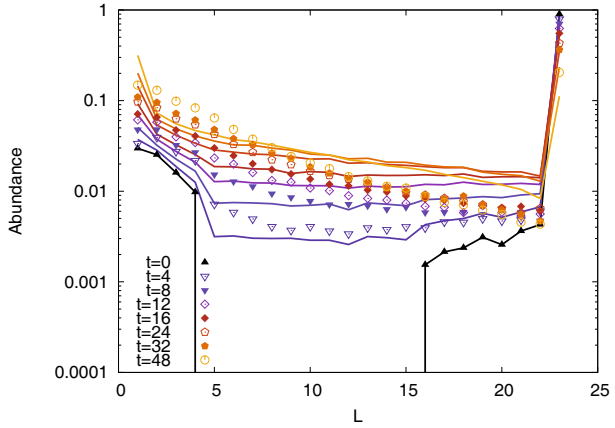

Fig. 8. Time evolution of the fragment length distribution as a function of time, for the simulation (lines) and the experiment (symbols). The simulation is fitted to the experimental data using two parameters: the cutting rate λ_c and the remodeling rate λ_r. The agreement is not very satisfactory.

As before we use a semiautomatic optimization of the two parameters. Using this procedure, we find the best parameters to be $\lambda_r = 0.42$ and $\lambda_c = 1$. It is interesting to note that the objective function is practically independent of λ_r over a wide range ($\lambda_r \lesssim 1$). This means that most likely, the system is actually in the steady state that we discussed earlier. It also means that we only have one true parameter in our system, which is the cutting rate λ_c.

The resulting time-evolving comparison between simulation and experiment is shown in fig. 8. It is obvious from the figure that the simulation fits the data rather badly ($d = 0.420$). One possible explanation is that some details in our model are not correct, and would have to be adjusted to produce a better fit. Another reason for the discrepancy might be that there are some additional effects that we did not account for, such as label-remodeler interaction or the emergence or destruction of higher-order geometrical structures of the nucleosomal array during remodeling.

5 Conclusions

We have presented new approaches to analyze experimental data on the accessibility of nucleosomal arrays during remodeling. In this endeavor, we have followed two different strategies. One is to stay close to the experimental data and to concentrate on models that are as simple as possible. The other approach is to introduce more detailed models, which were tested here for the ACF remodeler. For the approach using simple models, we found that the ISWI experimental data can be explained by assuming identical Poisson distributed cutting times for each individual restriction site, and no further interaction between the nucleosomes.

The ACF-type remodeler presents a more complicated picture. The simple ISWI model works very poorly when applied to the ACF experimental data. This is in a way expected, because it was already known that the ACF remodeler has the ability to position nucleosomes according to their distance to each other. A simple model with a lower number of steps close to the attached label works very well. This raises the question, where this asymmetry stems from. We have two main suggestions. One possibility is the interaction of the remodeler with the fluorescent label at one end of the DNA fragment, as has been observed before in other systems [47,48]. The other possibility concerns the asymmetric position of the AluI restriction sites with respect to the (equilibrium or starting) positions of the nucleosomes. By studying more detailed models we have shown that the latter effect can indeed cause asymmetries in the cutting probabilities. The degree of asymmetry is however not explained by our models, even when using a very detailed approach.

This work is part of the research programme of the Foundation for Fundamental Research on Matter (FOM), which is financially supported by the Netherlands Organisation for Scientific Research (NWO). PBB is grateful for support by the Deutsche Forschungsgemeinschaft via grant SFB594-A6 and BE1140/6. HK acknowledges support by the Elite Network of Bavaria.

References

1. K. Luger, A.W. Mäder, R.K. Richmond, D.F. Sargent, T.J. Richmond, Nature **389**, 251 (1997).
2. R. Blossey, H. Schiessel, FEBS J. **278**, 3619 (2011).
3. K.J. Polach, J. Widom, J. Mol. Biol. **254**, 130 (1995).
4. J.D. Anderson, J. Widom, J. Mol. Biol. **296**, 979 (2000).
5. J.D. Anderson, P.T. Lowary, J. Widom, J. Mol. Biol. **307**, 977 (2001).
6. G. Li, M. Levitus, C. Bustamante, J. Widom, Nat. Struct. Mol. Biol. **12**, 46 (2005).

7. L. Kelbauskas, N. Chan, R. Bash, J. Yodh, N. Woodbury, D. Lohr, Biochemistry **46**, 2239 (2007).
8. A. Gansen, A. Valeri, F. Hauger, S. Felekyan, S. Kalinin, K. Toth, J. Langowski, C.A.M. Seidel, Proc. Natl. Acad. Sci. U.S.A. **106**, 15308 (2009).
9. W.J.A. Koopmans, R. Buning, T. Schmidt, J. van Noort, Biophys. J. **97**, 195 (2009).
10. R. Prinsen, H. Schiessel, Biochimie **92**, 1722 (2010).
11. H.S. Tims, K. Gurunathan, M. Levitus, J. Widom, J. Mol. Biol. **411**, 430 (2011).
12. I. Jimenez-Useche, C. Yuan, Biophys. J. **103**, 2502 (2012).
13. S. Pennings, G. Meersseman, E.M. Bradbury, J. Mol. Biol. **220**, 101 (1991).
14. G. Meersseman, S. Pennings, E.M. Bradbury, EMBO J. **11**, 2951 (1992).
15. S. Pennings, G. Meersseman, E.M. Bradbury, Proc. Natl. Acad. Sci. U.S.A. **91**, 10275 (1994).
16. A. Flaus, T.J. Richmond, J. Mol. Biol. **275**, 427 (1998).
17. J.M. Gottesfeld, J.M. Belitsky, C. Melander, P.B. Dervan, K. Luger, J. Mol. Biol. **321**, 249 (2002).
18. S. Pisano, E. Marchioni, A. Galati, R. Mechelli, M. Savino, S. Cacchione, J. Mol. Biol. **369**, 1153 (2007).
19. A. Flaus, T. Owen-Hughes, Biopolymers **68**, 563 (2003).
20. H. Schiessel, J. Phys.: Condens. Matter **15**, R699 (2003).
21. H. Schiessel, J. Widom, R.F. Bruinsma, W.M. Gelbart, Phys. Rev. Lett. **86**, 4414 (2001).
22. I.M. Kulić, H. Schiessel, Biophys. J. **84**, 3197 (2003).
23. I.M. Kulić, H. Schiessel, Phys. Rev. Lett. **91**, 148103 (2003).
24. F. Mohammad-Rafiee, I.M. Kulić, H. Schiessel, J. Mol. Biol. **344**, 47 (2004).
25. A. Fathizadeh, A.B. Besya, M.R. Ejtehadi, H. Schiessel, Eur. Phys. J. E **36**, 21 (2013).
26. A. Flaus, D.M.A. Martin, G.J. Barton, T. Owen-Hughes, Nucl. Acids Res. **34**, 2887 (2006).
27. C.R. Clapier, B.R. Cairns, Annu. Rev. Biochem. **78**, 273 (2009).
28. A.E. Leschziner, Curr. Opin. Struct. Biol. **21**, 709 (2011).
29. G.J. Narlikar, R. Sundaramoorthy, T. Owen-Hughes, Cell **154**, 490 (2013).
30. P.D. Varga-Weisz, M. Wilm, E. Bonte, K. Dumas, M. Mann, P.B. Becker, Nature **388**, 598 (1997).
31. J.G. Yang, T.S. Madrid, E. Sevastopoulos, G.J. Narlikar, Nat. Struct. Mol. Biol. **13**, 1078 (2006).
32. L.R. Racki, J.G. Yang, N. Naber, P.D. Partensky, A. Acevedo, T.J. Purcell, R. Cooke, Y. Cheng, G.J. Narlikar, Nature **462**, 1016 (2009).
33. T.R. Blosser, J.G. Yang, M.D. Stone, G.J. Narlikar, X. Zhyang, Nature **462**, 1022 (2009).
34. S.E. Torigoe, D.L. Urwin, H. Ishii, D.E. Smith, J.T. Kadonaga, Mol. Cell **43**, 638 (2011).
35. A.-M. Florescu, H. Schiessel, R. Blossey, Phys. Rev. Lett. **109**, 118103 (2012).
36. P. Korber, P.B. Becker, Essays Biochem. **58**, 63 (2010).
37. G. Lanzani, H. Schiessel, EPL **97**, 38002 (2012).
38. V.K. Maier, M. Chioda, D. Rhodes, P.B. Becker, EMBO J. **27**, 817 (2008).
39. H. Klinker, F. Mueller-Planitz, R. Yang, I. Forné, C.-F. Liu, L. Nordenskiöld, P.B. Becker, PLoS ONE **9**, e88411 (2014).
40. A. Eberharter, S. Ferrari, G. Längst, T. Straub, A. Imhof, P. Varga-Weisz, M. Wilm, P.B. Becker, EMBO J. **20**, 3781 (2001).
41. X. He, H.-Y. Fan, G.J. Narlikar, R.E. Kingston, J. Biol. Chem. **281**, 28636 (2006).
42. P.T. Lowary, J. Widom, J. Mol. Biol. **276**, 19 (1998).
43. K.J. Polach, J. Widom, Methods Enzymol. **304**, 278 (1999).
44. P.D. Gregory, S. Barbaric, W. Hörz, Methods Mol Biol. **119**, 417 (1999).
45. C. Logie, C.L. Peterson, EMBO J. **16**, 6772 (1997).
46. G.J. Narlikar, M.L. Phelan, R.E. Kingston, Mol. Cell **8**, 1219 (2001).
47. A.R. Khaki, C. Field, S. Malik, A. Niedziela-Majka, S.A. Leavitt, R. Wang, M. Hung, R. Sakowicz, K.M. Brendza, C.J. Fischer, J. Mol. Biol. **400**, 345 (2010).
48. G. Al-Ani, K. Briggs, S.S. Malik, M. Conner, Y. Azumi, C.J. Fischer, Biochemistry **53**, 4334 (2014).
49. R. Kornberg, L. Stryer, Nucl. Acids Res. **16**, 6677 (1988).
50. E. Segal, Y. Fondufe-Mittendorf, L. Chen, A.C. Thaström, Y. Field, I.K. Moore, J.-P.Z. Wang, J. Widom, Nature **442**, 772 (2006).
51. P.D. Partensky, G.J. Narlikar, J. Mol. Biol. **391**, 12 (2009).
52. L. Tonks, Phys. Rev. **50**, 955 (1936).
53. G. Chevereau, L. Palmeira, C. Thermes, A. Arneodo, C. Vaillant, Phys. Rev. Lett. **103**, 188103 (2009).